

A Tri-Band Impedance Transformer Based Output Network for Efficient RF Power Amplifiers

Antra Saxena^{1, *} and Mohammad S. Hashmi²

Abstract—Design of a harmonically tuned RF Power Amplifier (PA) with enhanced efficiency and gain is presented in this paper. It makes use of a tri-band impedance transformer as a two-port output network for facilitating concurrent optimum fundamental and harmonic impedances at the drain terminal. The design is augmented by analytical formulations and analysis to identify the optimal impedance matching scenario at the fundamental, second harmonic, and third harmonic. A thorough analysis reveals that the proposed PA design scheme is very simple while maintaining the performance obtained from the load-pull. A prototype operating at a frequency of 3.5 GHz is developed on RO5880 using 10 W GaN HEMT. An excellent agreement between the measured and EM simulated results validates the proposed design technique.

1. INTRODUCTION

Power amplifier is an essential component required to convert DC into RF power in microwave devices. The overall performance of a wireless transmitter is highly reliant on the features, namely Power Added Efficiency (PAE), output power, gain, etc. of RF Power Amplifiers (PAs). Different classes are defined to enhance the efficiency of a power amplifier. By controlling the current conduction angle, the PAs operating as Class-A, B, AB, and C are defined. Theoretically, class-A amplifier can achieve maximum 50% drain efficiency with both current and voltage waveforms as sinusoidal. However, to increase the efficiency, the current and voltage waveforms need to be reshaped. To reshape the waveforms, drain voltage may contain a number of harmonics while maintaining current waveform as sinusoidal or vice-versa. This technique basically reduces the overlapping area between waveforms resulting in a new class of PAs, namely switched-mode (Class-D, Class-E) and harmonic-tuned PAs (Class-F or Class-F⁻¹) [1–5].

In the defined classes, the drain current and voltage waveforms are altered by terminating the harmonic load impedances such that they contain infinite number of harmonics. It is imperative to note that by avoiding overlap between voltage and current waveforms, power dissipation can be minimized, and theoretically drain efficiency can reach 100%. However, practically, it is not possible to alter infinite harmonics, but it is possible to achieve efficiency greater than 75% by controlling first three harmonics.

Also, it is well established that transistors must be driven in a nonlinear region of operation to achieve high PAE and output power. It is also widely acknowledged that highly efficient RFPA configurations such as switched-mode PAs are often constrained in the choice of the frequency of operation. This could be attributed to parasitic capacitance and inductance at the drain of the transistors which prevent operation as ideal switch [6]. A number of design techniques have been reported in the past decade to circumvent this issue, and some of them can be considered seminal [7–17]. In general, designs utilizing input harmonic terminations [7], broadband harmonic tuned approach [8], external harmonic injection [9], independent harmonic tuned output network [12], harmonic treatment

Received 29 July 2020, Accepted 15 October 2020, Scheduled 28 October 2020

* Corresponding author: Antra Saxena (antras@iiitd.ac.in).

¹ Department of Electronics and Communication at IIIT Delhi, New Delhi, India. ² School of Engineering and Digital Sciences, Nazarbayev University, Nur Sultan, Kazakhstan.

up to fourth order [13], concurrent dual-band harmonic-tuned [15], second harmonic tuned [16], harmonic tuned inverse Class-F using bare-die device [17], etc. have found wide acceptance as can be inferred from their use in commercial products.

In the past, different multi-band passive networks have been proposed operating at different frequencies concurrently including tri-band branch line coupler with open/short-circuit stubs [19], quad-band branch line coupler based on optimization compensation technique [20], tri-band impedance transformer based on virtual impedance [21], etc. This paper makes use of a reported tri-band design methodology [19], as a two-port output network, to match the optimal fundamental, second, and third harmonic impedances concurrently at the output of transistor. This technique provides a method for designing an output matching network using closed-form equations. The proposed design is augmented by analytical formulations for obtaining the requisite design parameters for the two-port output network. It is demonstrated that the incorporation of a two-port output network enhances the performance of harmonically tuned PAs with mathematical framework apart from reduction in the circuit complexity and form factor.

2. CIRCUIT DESIGN AND ANALYSIS

2.1. The Proposed Configuration

In harmonic tuned PAs, optimal terminations are required at the fundamental as well as the second and third harmonics [7–13]. For example, the design of the conventional Class-F/ F^{-1} power amplifiers entails proper short/open harmonic terminations at the current generator plane, followed by the fundamental match. Usually, the matching at harmonic frequencies requires intense optimization and can be quite tedious [11–13]. The proposed design scheme depicted in Fig. 1 envisages addressing this concern. It incorporates a tri-band impedance transformer at the output to match the fundamental and harmonic impedances with the load R_L .

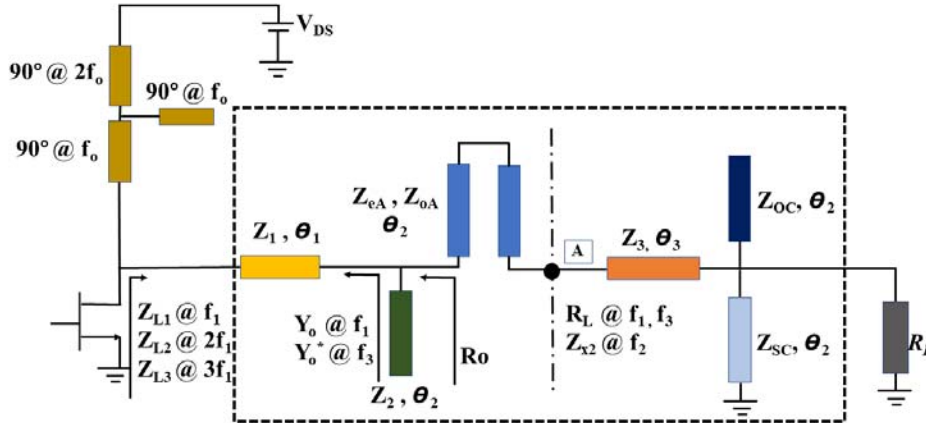


Figure 1. Schematic of the proposed two-port output network.

The two-port output network identified by the dashed box in Fig. 1 primarily serves to match the fundamental and harmonic impedances at the transistor's drain terminal to a resistive load R_L . Here, the output impedance is represented by Z_{L1} , Z_{L2} , and Z_{L3} at the fundamental f_1 , second f_2 , and third f_3 harmonics, respectively.

2.2. Analysis and Design

2.2.1. Drain Network

It is imperative to note that for matching the drain impedance at fundamental, second, and third harmonic frequencies to load resistance R_L , the drain biasing network should provide high impedance

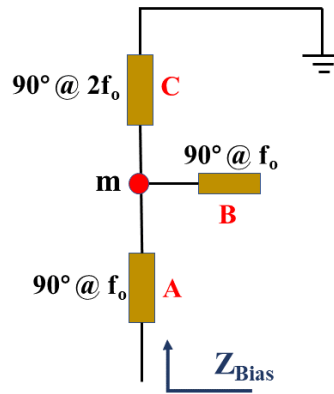


Figure 2. Drain bias network.

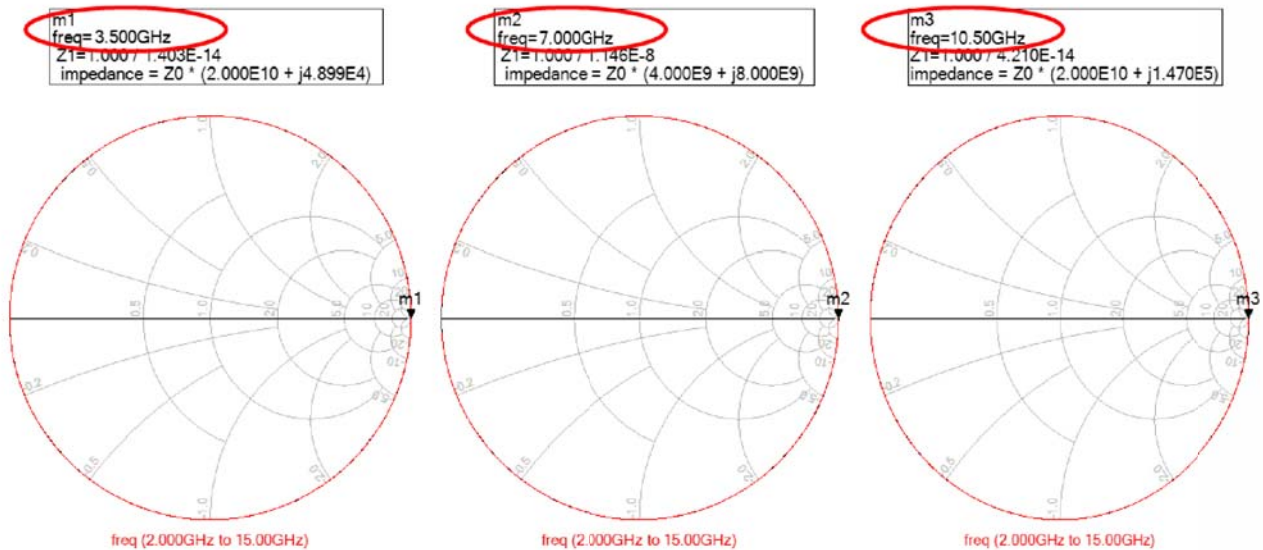


Figure 3. Impedance looking at the drain bias network at fundamental frequency, second and third harmonic.

at all three harmonics. The designed drain network shown in Fig. 2 is capable of providing infinite impedances at the designed fundamental frequency, its second and third harmonics as discussed.

At the fundamental frequency and third harmonic, Z_{Bias} in Fig. 2 will be open-circuit, since all transmission lines are quarter-wave, and node ‘m’ is at short-circuit because of transmission line ‘B’. Hence, transmission line will transfer short-circuit to open-circuit. Similarly, for second harmonic, node ‘m’ will be at open circuit because of transmission line C, and then transmission line A will see an open-circuit as shown in Fig. 3.

2.2.2. Output Matching Network

In Fig. 1, the output network is a tri-band impedance transformer designed using the concept discussed in [19]. It consists of a coupled-line dual-band impedance transformer [22] denoted by Z_{eA} , Z_{oA} , θ_2 and a dual-band transmission line-based L-network [23] indicated by Z_1 , θ_1 and Z_2 , θ_2 . It facilitates matching the device’s fundamental/harmonic impedances, $Z_{L1} = R_1 + jX_1$ at f_1 , $Z_{L2} = R_2 + jX_2$ at f_2 , and $Z_{L3} = R_3 + jX_3$ at $f_3 = 3f_1$, achieved using load-pull for optimal efficiency [18] and the load

impedance R_L .

First, the impedances Z_{L1} and Z_{L3} are transformed into complex conjugate, i.e., $Y_O|_{f_1} = Y_O^*|_{f_3}$, by the segment $[Z_1, \theta_1]$ of the L-network. Here, $Y_O = 1/Z_O = G_O + jB_O @ f_1$ and $G_O - jB_O @ f_3$. Subsequently, the susceptance B_O is cancelled by the dual-band stub $[Z_2, \theta_2]$ of the L-network. The parameters $[Z_1, \theta_1]$ and $[Z_2, \theta_2]$ are calculated using Eqs. (1) and (2), respectively [21]. The term $r_{31} = f_3/f_1$ is the frequency ratio.

$$Z_1 = \sqrt{R_1 R_3 + X_1 X_3 + \frac{X_1 + X_3}{R_1 + R_3} (R_1 X_3 - R_3 X_1)} \quad (1a)$$

$$\theta_1 = \frac{n\pi + \arctan \frac{Z_1(R_1 - R_3)}{R_1 X_3 - R_3 X_1}}{1 + r_{31}} \quad (1b)$$

$$\theta_2 = \frac{n\pi}{1 + r_{31}} = \frac{n\pi}{4} \quad (2a)$$

$$Z_2 = \frac{-j \cot \theta_2}{B_O} \text{ (Short)}, \quad Z_2 = \frac{j \tan \theta_2}{B_O} \text{ (Open)} \quad (2b)$$

The real part $R_O = 1/G_O$ is then matched with the load impedance, R_L , at f_1 and f_3 by the dual-band $\lambda/4$ coupled-line impedance transformer. The image impedance of the coupled line transformer, $Z_A = \sqrt{R_O R_L}$ [22], is related to its corresponding even- and odd-mode characteristic impedances Z_{eA} and Z_{oA} which are given in Eq. (3). Furthermore, in the process of matching at f_3 and f_1 , second harmonic impedance Z_{L2} gets transformed to a new value $Z_{X2} = G_{X2} + jB_{X2} @ f_2$, expressed in Eq. (4), at node A in Fig. 1.

$$Z_{eA} = Z_A \tan \theta_2 \text{ and } Z_{oA} = Z_A / \tan \theta_2 \quad (3)$$

$$Z_{X2} = Z_A^2 \left[\frac{(Z_1 + jZ_{L2} \tan \theta_1)}{(Z_1 Z_{L2} + jZ_1^2 \tan \theta_1)} \right] + j * \frac{\tan \theta_2}{Z_2} \quad (4)$$

At node A, as shown in Fig. 1, the value of impedances present at three different frequencies are as follows: $R_L @ f_1$ and f_3 , with $Z_{x2} @ f_2$. However, at the fundamental and third harmonic, the drain impedance is already matched to load impedance R_L , but $Z_{x2} @ f_2$ needs to be matched without disturbing the match at f_1 and f_3 . Thus, a transmission line with characteristic impedance $Z_3 = R_L$ with electrical length θ_3 is used [19]. Here, impedance Z_3 is equal to load resistance R_L , and hence matching at fundamental and third harmonic will remain the same, while transforming the $Z_{x2} @ f_2$ to a new value, which can be controlled by its electrical length θ_3 .

$$G_{X2} = \frac{1}{\left(\frac{R_L^3}{R_L^2 \tan^2 \theta_3 + R_L^3} \right) + \left(\frac{R_L^3 \tan^2 \theta_3}{R_L^2 \tan^2 \theta_3 + R_L^3} \right)} \quad (5a)$$

$$B_{X2} = \frac{1}{\left(\frac{R_L^3 \tan \theta_3}{R_L^2 \tan^2 \theta_3 + R_L^3} \right) - \left(\frac{R_L^2 Z_3 \tan 2\theta_3}{R_L^2 \tan^2 \theta_3 + R_L^3} \right)} \quad (5b)$$

It can be seen from Eqs. (5a) and (5b), by calculating the value of θ_3 the real part G_{X2} can be set equal to $1/R_L$. Thus, at second harmonic, the real part is matched perfectly with the load. However, the susceptance generated by this transmission line needs to be canceled without disturbing the matching at fundamental and third harmonic. Thus, a combination of open and short circuit stubs with characteristic impedances Z_{OC} and Z_{SC} respectively is utilized. This network should be capable of canceling the susceptance generated at second harmonic while providing infinite admittance at fundamental and third harmonic. To maintain that the admittance seen by fundamental and third harmonic should be infinite, the relation $Z_{OC} = Z_{SC} \tan^2 \theta_2$ should hold. However, the impedance provided by the stub network should cancel the susceptance $B_{X2} @ f_2$. The expression for calculating the impedance of the stub network is given below:

$$B_{X2} = -jY_{OC} \cot(x\theta_2) + jY_{SC} \tan(x\theta_2) \quad (6)$$

Here, x is defined as f_2/f_1 , while θ_2 is defined at the fundamental frequency. Substituting the value of $Y_{OC} = Y_{SC} \cot^2 \theta_2$ in Eq. (6), the characteristic impedances of short-circuit stub Z_{SC} and hence open-circuit Z_{OC} are given in Eqs. (7a) and (7b), respectively.

$$Z_{SC} = \frac{\cot^2 \theta_2 \cot(x\theta_2) + \tan(x\theta_2)}{B_{X2}} \quad (7a)$$

$$Z_{OC} = Z_{SC} \tan^2 \theta_2 \quad (7b)$$

This completes the mathematical derivation of the tri-band impedance transformer.

3. CASE STUDY AND EXPERIMENTAL EVALUATION

To validate the theoretical proposition, first, the standard 10 W GaN HEMT was biased at a gate voltage of $V_{GS} = -2.7$ V and drain voltage of $V_{DS} = 28$ V for the drain current of $I_D = 63$ mA. Then load-pull simulation was carried out for maximized efficiency by tuning the first two harmonics, and the achieved fundamental and harmonic impedances are listed in Table 1. Then an output two-port network is designed using the concept presented in Section 2. All the parameters are chosen so that they remain within the realizable limits of 20–150 Ω , and it is readily inferred from the parameters listed in Table 2.

Table 1. Optimum impedances at the drain of transistor.

Frequency	Output Impedances (Ω)
$f_1 = 3.5$ GHz	$10.27 + j1.245$
$f_2 = 7.0$ GHz	$1.1 + j1.5$
$f_3 = 10.5$ GHz	$7.75 + j14.35$

Table 2. Design parameters of matching network.

L-Network	Coupled-Line Transformer	Transformation Network
$Z_1 = 26.44 \Omega$	$Z_e = 55 \Omega$	$Z_3 = 50 \Omega$
$Z_2 = 148 \Omega$	$Z_o = 50 \Omega$	$\theta_3 = 60.53^\circ$
$\theta_1 = 75^\circ$	$\theta_2 = 45^\circ$	$Z_{OC} = 133 \Omega$
—	—	$Z_{SC} = 82 \Omega$

It is interesting to investigate the impedance trajectories. Fig. 4 illustrates the co-simulated trajectories of the fundamental, second, and third harmonic impedances for a frequency range of 3.4–3.7 GHz. The impedances lying on these trajectories correspond to drain efficiency of more than 50%. Furthermore, the impact of the transmission line parameters on the overall design is also significant. The relationship of the optimal efficiency related to the electrical length of θ_1 is given in Fig. 5. The drain efficiency is maximum when θ_1 falls within the shaded region. At the design frequency of 3.5 GHz, it is evident that θ_1 should be approximately 75° , which is close to the value obtained for the designed network given in Table 2. The impact of θ_2 is also significant on the achievable drain efficiency, as can be inferred from Fig. 6. The shaded region is earmarked for optimal efficiency, and it is in perfect agreement with the data in Table 2.

Furthermore, the variation of drain efficiency with the drain impedances at fundamental frequency is also an important aspect. In this context, the variation of drain efficiency with load is depicted in Fig. 7. Apparently, the boundary of impedance ratio at fundamental frequency (i.e., Z_L/Z_S) for maintaining efficiency above 60% is between 0.1 and 0.5. It can also be inferred from Fig. 7 that in this case, the maximum efficiency is achievable for the fundamental impedance, i.e., Z_{L1} , of $10.27 + j * 1.2 \Omega$ obtained from load-pull.

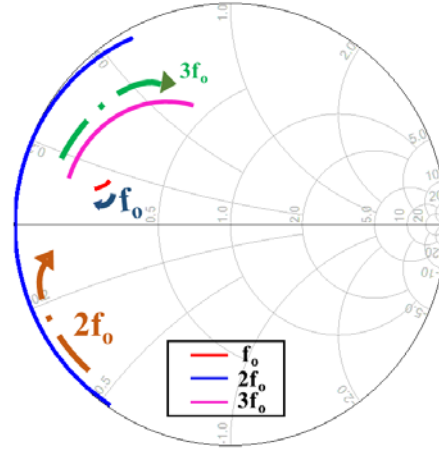


Figure 4. Impedance trajectories at the drain of the transistor.

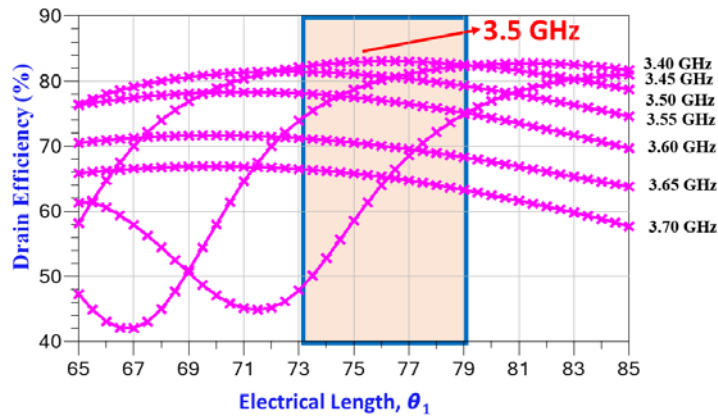


Figure 5. Dependence of drain efficiency on θ_1 for different frequency.

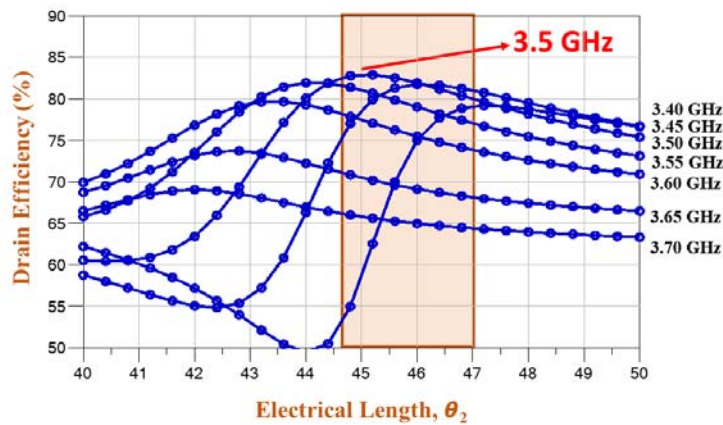


Figure 6. Dependence of drain efficiency on θ_2 for different frequency.

The schematic of the measurement setup is shown in Fig. 8. Keysight (MXG N5182B) and Vector Network Analyzer (PXA N9030B) are used for generating and receiving the signal, respectively. The developed PA prototype on an RO5880 substrate ($\epsilon_r = 2.2$, thickness 1.575 mm, 1 oz Cu) using 10 W GaN Wolfspeed GaN HEMT, shown in Fig. 9, is measured at the design frequency of 3.5 GHz. The

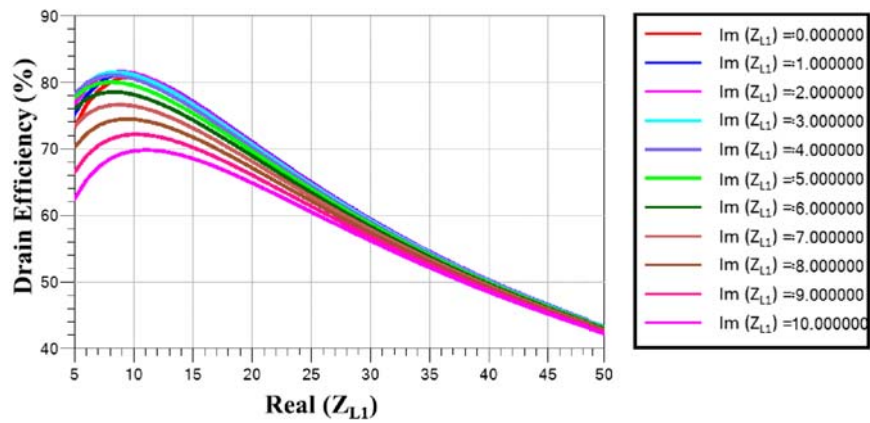


Figure 7. Drain efficiency vs fundamental load *Real — Real part of impedance (Z_{L1}) @ fundamental frequency, *Im — Imaginary part of impedance (Z_{L1}) @ fundamental frequency.

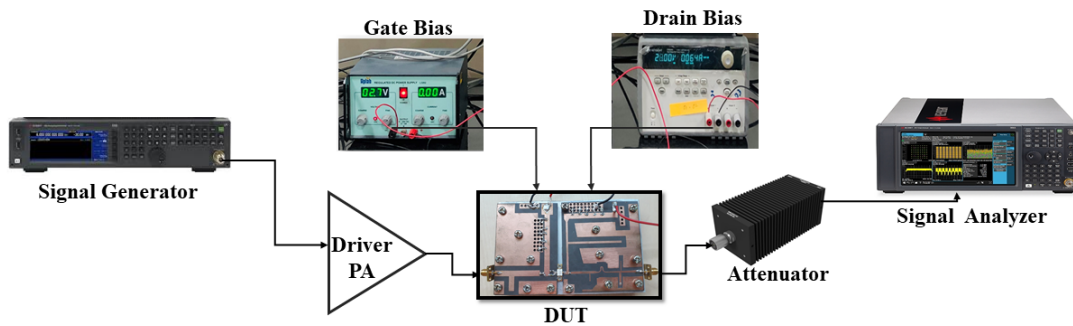


Figure 8. Schematic of the measurement setup.

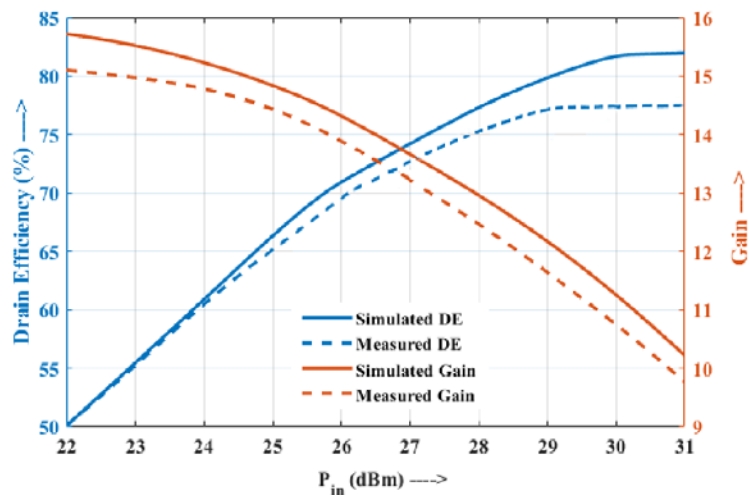


Figure 9. Drain efficiency and gain for input power sweep.

drive power is swept from 22–31 dBm, and then PAE, DE, and gain are measured, which are plotted in Figs. 9 and 10. For an input power of 30 dBm, the maximum measured PAE and DE are 73.8% and 77.3%, respectively, while the gain is 10.4 dB. Also, current and voltage waveforms at the transistor’s intrinsic plane are presented in Fig. 11. These are in good agreement with the corresponding simulation

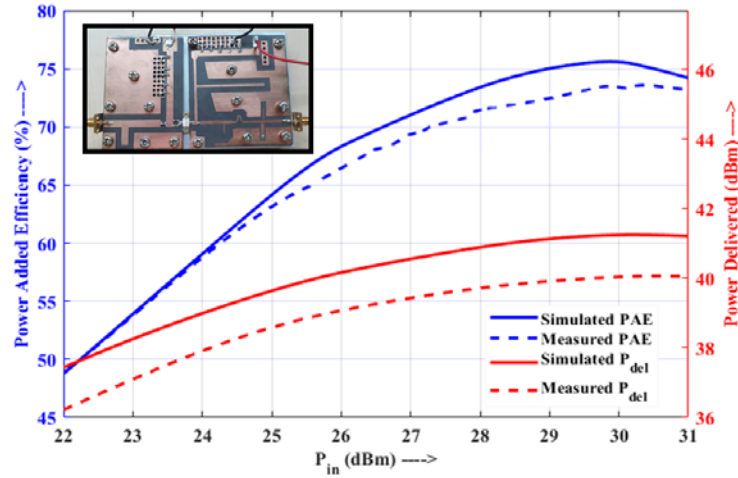


Figure 10. The prototype, PAE and power delivered for input power sweep.

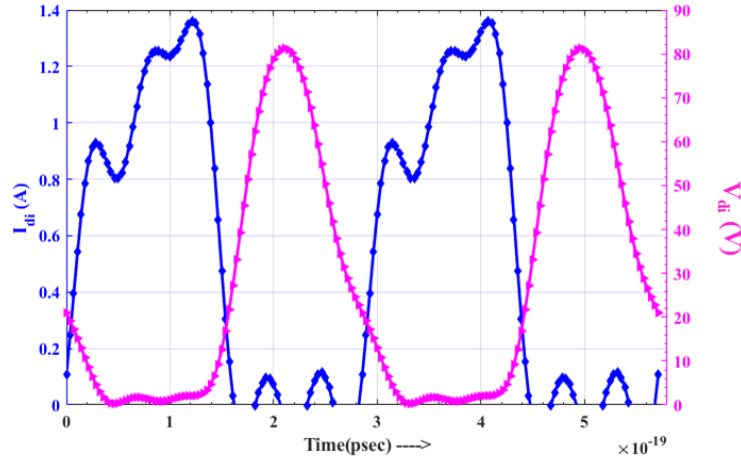


Figure 11. Voltage and current waveforms at the intrinsic plane of transistor.

Table 3. Comparison with the previous 3.5 GHz PA design.

References	Transistor Used	Frequency (GHz)	Pout (dBm)	PAE (%)	DE (%)
EuMC ⁺ [24]	GaN HEMT	3.5	40.5	72	79
EuMC [16]	GaN HEMT	3.5	35.3	57.7	69
TMTT ⁺ [10]	GaN HEMT	3.5	40.2	70	75.8
TMTT [2]	GaN HEMT	3.54	55	63	70
This Work	GaN HEMT	3.5	40.4	73.8	77.3

+ Class-E PA

results. Finally, the achieved results for the proposed design are compared with previously reported designs at 3.5 GHz in Table 3. It demonstrates that the proposed design technique could be a potential alternative with the achieved results compared favorably to the reported designs.

4. CONCLUSION

A new PA design approach based on a tri-band impedance transformer as a two-port matching network has been proposed. This technique simplifies the design procedure for controlling fundamental, second and third harmonics because of closed-form equations. The design is supported by analytical formulations, which assist in easy prototyping. The proposed technique has been evaluated experimentally using Wolfspeed 10 W GaN HEMT, and it has been shown that the achieved results are in good agreement with EM simulation results.

ACKNOWLEDGMENT

The authors acknowledge Dr. Karun Rawat and his lab members at IIT Roorkee (India) for assistance with the measurements and validation.

REFERENCES

1. Grebennikov, A. and N. O. Sokal, *Switchmode RF Power Amplifiers*, Newnes, Newton, MA, USA, 2007.
2. Kim, J. H., G. D. Jo, J. F. Oh, Y. H. Kim, K. C. Lee, and J. H. Jung, "Modeling and design methodology of high-efficiency class-F and class-F⁻¹ power amplifiers," *IEEE Trans. Microw. Theory Techn.*, Vol. 59, No. 1, 153–165, 2011.
3. Tanany, A. A., A. Sayed, and G. Boeck, "Analysis of broadband GaN switch mode class-E power amplifier," *Progress In Electromagnetics Research Letters*, Vol. 38, 151–160, 2013.
4. Raab, F. H., "Maximum efficiency and output of class-F power amplifiers," *IEEE Trans. Microw. Theory Techn.*, Vol. 49, No. 6, 1162–1166, 2001.
5. Xu, Y., J. Wang, and X. Zhu, "Analysis and implementation of inverse class-F power amplifier for 3.5 GHz transmitters," *Proc. Asia-Pacific Microw. Conf.*, 410–413, 2010.
6. Lee, Y. S. and Y. H. Jeong, "A high-efficiency class-E GaN HEMT power amplifier for WCDMA applications," *IEEE Microwave and Wireless Components Letters*, Vol. 17, No. 8, 622–624, 2007.
7. Gao, S., P. Butterworth, S. Ooi, and A. Sambell, "High-efficiency power amplifier design including input harmonic termination," *IEEE Microwave and Wireless Components Letters*, Vol. 16, No. 2, 81–83, 2006.
8. Liu, G., S. Li, Z. Cheng, H. Feng, and Z. Dong, "High efficiency broadband GaN HEMT power amplifier based on harmonic tuned matching approach," *International Journal of RF and Microwave Computer Aided Engineering*, Vol. 30, No. 2, e22097, 2020.
9. Dani, A., M. Roberg, and Z. Popovic, "PA efficiency and linearity enhancement using external harmonic injection," *IEEE Trans. Microw. Theory Techn.*, Vol. 60, No. 12, 4097–4106, 2012.
10. Jee, S., J. Moon, J. Kim, J. Son, and B. Kim, "Switching behavior of class-E power amplifier and its operation above maximum frequency," *IEEE Trans. Microw. Theory Techn.*, Vol. 60, No. 1, 89–98, Dec. 2011.
11. Lee, Y. S., M. W. Lee, and Y. H. Jeong, "High-efficiency class-F GaN HEMT amplifier with simple parasitic-compensation circuit," *IEEE Microwave and Wireless Components Letters*, Vol. 18, No. 1, 55–57, 2008.
12. Banerjee, D., A. Saxena, and M. Hashmi, "A novel independent harmonic tuned two port output network for efficiency enhanced RF power amplifiers," *Microwave and Optical Technology Letters*, 2020, doi: 10.1002/mop.32615.
13. Kamiyama, M., I. Ryo, and H. Kazuhiko, "5.65 GHz high-efficiency GaN HEMT power amplifier with harmonics treatment up to fourth order," *IEEE Microwave and Wireless Components Letters*, Vol. 22, No. 6, 315–317, 2012.
14. Saad, P., H. M. Nemati, K. Andersson, and C. Fager, "Highly efficient GaN-HEMT power amplifiers at 3.5 GHz and 5.5 GHz," *Proc. IEEE WAMICON Conf.*, 1–4, 2011.

15. Colantonio, P., F. Giannini, R. Giofre, and L. Piazzon, "A design technique for concurrent dual-band harmonic tuned power amplifier," *IEEE Trans. Microw. Theory Techn.*, Vol. 56, No. 11, 2545–2555, 2008.
16. El Maazouzi, L., P. Colantonio, A. Mediavilla, and F. Giannini, "A 3.5 GHz 2nd harmonic tuned PA design," *IEEE European Microw. Conf. (EuMC)*, 1090–1093, 2009.
17. Saad, P., C. Fager, H. M. Nemati, H. Cao, H. Zirath, and K. Andersson, "A highly efficient 3.5 GHz inverse class-F GaN HEMT power amplifier," *Inter. Journal of Micro. Wireless Techno.*, Vol. 2, Nos. 3–4, 317–24, 2010.
18. Ghannouchi, F. M. and M. S. Hashmi, *Load-pull Techniques with Applications to Power Amplifier Design*, Springer Series in Advanced Microelectronics, 2013.
19. Lin, F., C. X. Qing, and L. Zhe, "A novel tri-band branch-line coupler with three controllable operating frequencies," *IEEE Microwave and Wireless Components Letters*, Vol. 20, No. 12, 666–668, 2010.
20. Piazzon, L., P. Saad, P. Colantonio, F. Giannini, K. Andersson, and C. Fager, "Branch-line coupler design operating in four arbitrary frequencies," *IEEE Microwave and Wireless Components Letters*, Vol. 22, No. 2, 67–69, 2012.
21. Banerjee, D., A. Saxena, and M. S. Hashmi, "A novel concept of virtual impedance for high frequency tri-band impedance matching networks," *IEEE Trans. Circuits Syst. II, Exp. Briefs*, Vol. 65, No. 9, 1184–1188, 2018.
22. Tang, X. and K. Mouthaan, "Compact dual-band power divider with single all pass coupled lines sections," *IET Elect. Lett.*, Vol. 46, No. 10, 688–689, 2010.
23. Maktoomi, M. A., V. Panwar, M. S. Hashmi, and F. M. Ghannouchi, "A dual-band matching network for frequency-dependent complex loads suitable for dual-band RF amplifiers," *IEEE Inter. Microw. RF Conf. (IMaRC)*, 88–91, 2014.
24. Lee, M. W., Y. S. Lee, and Y. H. Jeong, "A high-efficiency GaN HEMT hybrid class-E power amplifier for 3.5 GHz WiMAX applications," *IEEE European Microw. Conf. (EuMC)*, 436–439, 2008.